# Elastic-plastic Rayleigh-Taylor instability at a cylindrical interface

A. R. Piriz* and S. A. Piriz
*Instituto de Investigaciones Energéticas, ETSII, and CYTEMA, Universidad de Castilla–La Mancha, 13071 Ciudad Real, Spain*

N. A. Tahir
*GSI Helmholtzzentrum für Schwerionenforschung Darmstadt, Planckstrasse 1, 64291 Darmstadt, Germany*

(Received 20 May 2021; accepted 20 August 2021; published 7 September 2021)

The boundaries of stability are determined for the Rayleigh-Taylor instability at a cylindrical interface between an ideal fluid in the interior and a heavier elastic-plastic solid in the outer region. The stability maps are given in terms of the maximum dimensionless initial amplitude $\xi_{th}^*$ that can be tolerated for the interface to remain stable, for any particular value of the dimensionless radius $B$ of the surface, and for the different spatial modes $m$ of the perturbations. In general, for the smallest dimensionless radius and larger modes $m$, the interface remains stable for larger values of $\xi_{th}^*$. In particular, for $m > 1$ and $B \to 0$, it turns out $\xi_{th}^* \to 1$, and a cylindrical geometry equivalent to Drucker's criterion is found, which indeed ends up being independent of the interface geometry.

DOI: 10.1103/PhysRevE.104.035102

## I. INTRODUCTION

Rayleigh-Taylor instability (RTI) in elastic and elastic-plastic (EP) media is of great relevance to many problems in high energy density (HED) physics, either because it plays a crucial role in determining the performance of the experiments [1–8] or because it is used as a tool for probing the mechanical properties of matter under extreme conditions of pressure, strain, and strain rate [9–18]. Although RTI in solids has been studied since Miles presented an approximate theoretical analysis of the instability in accelerated plates [19], the field has only significantly progressed during the past two decades in which a number of experiments on HED material science have been performed, thus stimulating the research by means of numerical simulations and theory [11,12,20–24]. Nevertheless, all the studies have concentrated so far on the RTI in planar surfaces by investigating different aspects related to the effect of the elastic properties [22], the finite thickness of the solid medium [25–28], and the presence of magnetic fields [29,30].

Besides, the more complex problem involving EP solids has been scarcely investigated by theory, and it has been done by analyzing the problem for semi-infinite media as a first step [20] and later for media with arbitrary thickness [31]. Very recently, a few experiments have been reported in which elastic or EP soft matter is used [32–35] and therefore HED is not involved, so much more friendly laboratory conditions are present. These experiments have the potential to contribute significantly to the understanding of RTI in solids since the physical processes are analogous while the mechanical properties of the material can be known in advance with rather good accuracy.

The above-mentioned theoretical works on RTI in EP solids were performed by assuming that the mechanical properties can be treated in such a manner that initially the material behaves as a purely elastic medium and that this phase is followed by one in which the medium behaves like a rigid-plastic solid. In addition, according to the classical theory of plasticity, this latter phase is considered as irrotational [36]. The good agreement of this model with two-dimensional (2D) numerical simulations [20,31] and with experimental results [35] suggests that it is a reasonably good way to deal with the problem by using theoretical tools and that consequently it could also be used in the study of the RTI at a cylindrical interface, such as we do in the present work.

In fact, one of the main motivations of our work has been the analysis of the performance of the Laboratory Planetary Science (LAPLAS) experimental setup on HED physics to be realized at the Facility for Ion and Antiproton Research, presently under construction at the GSI Helmholtzzentrum Darmstadt (Germany). In this experiment, an intense heavy ion beam will deposit part of its energy in an annular region that surrounds a solid cylindrical shell [1,37–44]. Then the expansion of this absorber region drives the implosion of the shell, thus compressing the sample in the interior, which is driven to HED conditions. Typical material samples under consideration are Fe, $H_2O$, and $H_2$, with which it is expected that LAPLAS will enable access to the core conditions of rocky and gaseous planets in the laboratory.

The planar geometry studies we have performed so far are appropriate for describing the RTI evolution at the external surface of the shell during the implosion phase, when the shell radius is still considerably large. However, at the stagnation phase, after the acceleration is reversed, the internal interface becomes unstable and curvature effects of the surface will be of relevance. Therefore, for the study of RTI in such a situation we can consider that, during the phase of maximum deceleration when RTI is more dangerous (Fig. 1), the shell's

*roberto.piriz@uclm.es

 

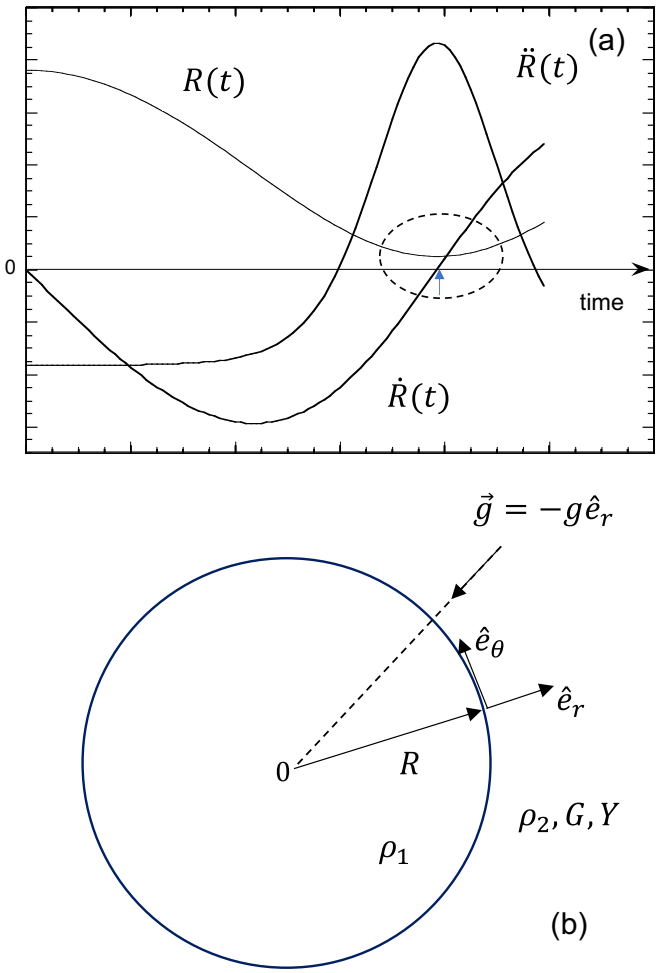


FIG. 1. Schematic of (a) the time evolution of the radius $R(t)$, velocity $\dot{R}(t)$, and acceleration $\ddot{R}(t)$ of the shell's internal surface and (b) the cylindrical interface between the ideal fluid in the interior and the elastic-plastic medium in the outer region.

internal surface is practically at rest and stress-free. Then we can neglect the convergence, or Bell-Plesset effect, and compression effects during the stagnation phase. Of course, convergence and compression effects are dominant during the previous implosion phase, and they determine the initial conditions for the RTI during the stagnation phase we are studying. This previous implosion phase is Rayleigh-Taylor (RT) stable most of the time, and the effects of the mechanical properties of the involved media during such a stage will be different than during the stagnation phase. Consequently, the implosion phase must be analyzed separately from the RT unstable stagnation phase. A similar approach was recently adopted in Refs. [45,46] involving viscous media, by following the pioneer work by Chandrasekhar [47], and also in Ref. [48] with elastic and viscous media.

In the present work we will determine the stability boundaries for the RTI on a cylindrical interface between an interior ideal fluid and an infinite EP solid medium in the outer region. This will allow us to know what the maximum perturbation amplitude is that can be tolerated at the beginning of the stagnation phase in order to ensure the interface stability at this later phase.

Our aim is to evaluate the effects of the curvature of the interface on the stability quality of a cylindrical implosion during the stagnation phase, under conditions in which the imploding payload retains its EP mechanical properties, as is the case of the LAPLAS experiment [37–44]. For this, we will follow a strategy similar to the one developed in Refs. [31,35] in order to analyze the effect of the surface curvature.

## II. LINEAR INSTABILITY ANALYSIS

We consider a cylindrical cavity of radius $R$ filled with an ideal fluid of density $\rho_1$ surrounded by an infinite EP medium of density $\rho_2 > \rho_1$ that occupies the region $r \geqslant R$ and with mechanical properties that can be characterized by constants shear modulus $G$ and yield strength $Y$ (Fig. 1). Both media are assumed to be incompressible and the whole system is subjected to a uniform gravity acceleration $\vec{g} = -g\hat{e}_r = -\vec{\nabla}\varphi$, where $\hat{e}_r$ is the unity vector in the radial direction and $\varphi$ is the gravitational potential. We restrict ourselves to the 2D case in which the interface is radially perturbed.

The equations governing the process are the mass and momentum conservation for incompressible continuous media

$$\vec{\nabla} \cdot \vec{v}_n = 0, \tag{1}$$

$$\rho_n \frac{d\vec{v}_n}{dt} = -\vec{\nabla} p_n + \rho_n \vec{g} + \vec{\nabla} \cdot \vec{\vec{\sigma}}_n, \tag{2}$$

where $n = 1, 2$ indicate the inner and outer media, respectively, $p_n$ is the hydrostatic pressure, $\vec{\vec{\sigma}}_n$ is the deviatoric part of the stress tensor $\vec{\vec{\Sigma}}_n = -p_n \vec{\vec{I}} + \vec{\vec{\sigma}}_n$, and $\vec{\vec{I}}$ is the identity tensor. In addition, the material derivative of any magnitude $M$ is

$$\frac{dM}{dt} = \frac{\partial M}{\partial t} + \vec{v}_n \cdot \vec{\nabla} M = 0. \tag{3}$$

The linearized equations are obtained as in Refs. [29–31,35] by writing every magnitude $M$ as $M = M_0 + \delta M$, where $M_0$ is the equilibrium value and $\delta M \ll M_0$ is the perturbation. In this manner, we get

$$\vec{\nabla} \cdot (\delta \vec{v}_n) = 0, \tag{4}$$

$$\rho_n \frac{\partial (\delta \vec{v}_n)}{\partial t} = -\vec{\nabla}(\delta p_n + \rho_n \delta \varphi_n) + \vec{\nabla} \cdot \vec{\vec{S}}_n, \tag{5}$$

where $\delta\varphi_n = \rho_n g \eta_{rn}$ ($\eta_{rn}$ is the radial component of the displacement $\vec{\eta}_n$ and $\dot{\vec{\eta}}_n = \delta \vec{v}_n$, where the overdot denotes time derivative) and we have defined $\delta\vec{\vec{\sigma}}_n \equiv \vec{\vec{S}}_n$. For the inner ideal fluid we have $\vec{\vec{S}}_1 = 0$, and for the solid medium in the exterior we assume, like in Refs. [31,35], that for the smallest strains it behaves like a perfectly elastic Hookean (linear) solid, so that

$$\frac{\partial \vec{\vec{S}}}{\partial t} = 2G\dot{\vec{\vec{e}}}, \quad \vec{\vec{e}} = \tfrac{1}{2}\left(\vec{\nabla}\vec{\eta} + \vec{\nabla}\vec{\eta}^{\,T}\right), \tag{6}$$

where $\vec{\vec{e}}$ is the strain tensor and the superscript $T$ indicates the transpose tensor. Instead, for the largest strains, the medium behaves like a perfectly rigid-plastic solid and the deviatoric

tensor is given by the von Mises flow rule

$$\vec{\vec{S}} = \sqrt{\frac{2}{3}} \frac{\dot{\vec{\vec{e}}}}{\|\dot{\vec{\vec{e}}}\|} Y. \tag{7}$$

Since the deviatoric tensor only exists for the solid medium, we have dropped the subscript of $\vec{\vec{S}}$ in Eqs. (6) and (7) and taken $\vec{\vec{S}}_2 \equiv \vec{\vec{S}}$.

It is worth mentioning that the von Mises flow rule indicates the moment at which the solid becomes plastic first at the interface. However, the transition of the instability from the regime ruled by the elastic properties to the one dominated by the plastic properties actually requires overcoming the intermediate phase of contained plastic flow in which the plastic region is not sufficiently extended to affect the RTI evolution [20,31,35,49–51]. This intermediate phase should actually be assimilated to the elastic regime until the occurrence of the plastic collapse so that the RTI plastic regime will start when the stress is indeed somewhat larger than the value given by Eq. (7).

### A. Elastic phase

#### *1. Displacement field*

The instability growth rate in a cylindrical interface surrounded by an elastic medium has been recently obtained by Sun *et al.* [48]. However, for the present purpose of determining the boundaries of stability, we need to find the oscillation frequencies of the interface in the complementary stable regime. Therefore, we will derive here the dispersion relation for such frequencies and, as in Refs. [27,31,35], we will use the Helmholtz decomposition for the displacement field in the solid medium

$$\vec{\eta}_2 = \vec{\nabla}\phi_2 + \vec{\nabla} \times \vec{\psi}_2, \tag{8}$$

where $\phi_2$ and $\vec{\psi}_2 = \psi_2 \hat{e}_z$ are the Lamé scalar and vector potentials, respectively. Introducing Eq. (8) into Eqs. (4) and (5), we obtain the equations

$$\nabla^2 \phi_n = 0, \tag{9}$$

$$\vec{\nabla}\left(\frac{\partial^2 \phi_n}{\partial t^2} + \frac{\delta p_n}{\rho_n} + \delta\varphi_n\right) + \vec{\nabla}\left(\frac{\partial^2 \psi_n}{\partial t^2} - \frac{G}{\rho_n}\nabla^2\psi_n\right)\hat{e}_z = 0, \tag{10}$$

where, for the ideal medium in the region $0 \leqslant r \leqslant R$, we have $\psi_1 = 0$.

The degree of freedom introduced by the vector potential allows for the choice of a convenient gauge, so the potential functions can be chosen in such a manner that Eq. (10) is split into the two equations

$$\rho_n \frac{\partial^2 \phi_n}{\partial t^2} + \delta p_n + \rho_n g \eta_{rn} = 0, \tag{11}$$

$$\rho_2 \frac{\partial^2 \psi_2}{\partial t^2} = G\nabla^2 \psi_2. \tag{12}$$

In polar coordinates, Eq. (9) leads to the following forms for the potentials $\phi_n$ in each region, internal and external, respectively:

$$\phi_1 = a_1 r^m \cos m\theta, \tag{13}$$

$$\phi_2 = \frac{a_2}{r^m} \cos m\theta, \tag{14}$$

where $m$ corresponds to the set of positive integers numbers and we have already imposed that the potentials $\phi_1$ and $\phi_2$ satisfy, respectively, the vanishing boundary conditions at $r = 0$ and for $r \to \infty$. In addition, these potentials are defined only to within an arbitrary additive function of time. Similarly, by solving Eq. (12) in the usual manner by separation of variables into polar coordinates, we find that the solution is of the form $\psi_2 = b(t)u(r)\sin m\theta$ and that the radial component $u(r)$ satisfies the Bessel equation

$$\frac{d^2u}{dr^2} + \frac{1}{r}\frac{du}{dr} + \left(q_m^2 - \frac{m^2}{r^2}\right)u = 0, \tag{15}$$

where

$$q_m = \sqrt{\frac{\rho_2 \omega_{mj}^2}{G}}, \tag{16}$$

with $\omega_{mj}$ all the possible oscillation frequencies, denoted by the subscript $j$ that will result from the solution of the dispersion relation for each particular mode $m$.

As it is well known, the general solution of Eq. (15) is given by the linear combination of the Bessel functions $J_m(q_m r)$ and $Y_m(q_m r)$ of the first and the second kind, respectively,

$$u(r) = A_1 J_m(x) + A_2 Y_m(x), \quad x = q_m r, \tag{17}$$

where $A_1$ and $A_2$ are constants to be determined by the boundary conditions at the interface and far from it, for $x \to \infty$. It is worth noting that in such a limit both $J_m(x)$ and $Y_m(x)$ vanish identically and therefore such a condition does not allow for determining a unique solution. In fact, in that limit, we have [52]

$$J_m(x) = \sqrt{\frac{2}{\pi x}}\cos(x - x_1), \quad Y_m(x) = \sqrt{\frac{2}{\pi x}}\sin(x - x_1), \tag{18}$$

with $x_1 = (m+1)\frac{\pi}{4}$. Then, in order to find a unique solution, we need to appeal to Sommerfeld's radiation condition [53], which sets that in a semi-infinite region ($r > R$) only outgoing waves ($\sim e^{ix}$) can exist and consequently the solution of Eq. (12) must be given by the Hankel function of the first kind $H_m(x)$ defined by the linear combination

$$H_m = J_m + iY_m, \quad i = \sqrt{-1}. \tag{19}$$

In this manner the incoming waves ($e^{-ix}$) are eliminated and the nonexistence of backward radiation from infinity is guaranteed. Then it turns out that

$$\psi_2 = bH_m(x)\sin m\theta. \tag{20}$$

In Eqs. (13), (14), and (20), $a_1$, $a_2$, and $b$ are time functions such that

$$a_1 \propto a_2 \propto b \propto F(t) = \sum_j Q_j e^{\omega_{mj} t}, \tag{21}$$

with $Q_j$ being constants that will be determined by the boundary conditions on the interface.

#### 2. Dispersion relation for the stable cases

In order to find the dispersion relation yielding all the possible oscillation frequencies $\omega_{mj}$ for the stable cases, we must impose the boundary conditions at $r = R$, namely, the continuity of the radial velocity and of the tangential and normal stresses

$$\delta v_{1r}(R) = \delta v_{2r}(R) = \dot{\eta}_a(\theta, t, R) = \dot{\xi}(t)\cos m\theta, \quad (22)$$

$$S_{r\theta}(R) = 0, \quad (23)$$

$$-\delta p_1(R) = -\delta p_2(R) + S_{rr}(R), \quad (24)$$

where $\delta p_n$ are given by Eq. (11) and we have the following expressions for $\dot{S}_{r\theta}(r)$ and $\dot{S}_{rr}(r)$:

$$\dot{S}_{r\theta}(r) = G\left[r\frac{\partial}{\partial r}\left(\frac{\delta v_{2\theta}}{r}\right) - \frac{1}{r}\frac{\partial(\delta v_{2r})}{\partial\theta}\right], \quad (25)$$

$$\dot{S}_{rr}(r) = 2G\frac{\partial(\delta v_{2r})}{\partial r}. \quad (26)$$

Then the previous boundary conditions yield the set of linear equations

$$\dot{a}_1 R^m = -\frac{\dot{a}_2}{R^m} + \dot{b}H_m, \qquad m\dot{a}_1 R^{m-1} = \dot{\xi}, \quad (27)$$

$$\frac{2m(m+1)}{R^m}\dot{a}_2 = -\dot{b}[2xH_{m-1} + x^2 H_m - 2m(m+1)H_m], \quad (28)$$

$$\rho_2\frac{\ddot{a}_2}{R^m} + \rho_2 g\left(-\frac{m}{R^{m+1}}a_2 + \frac{m}{R}bH_m\right) + C_0 + 2G\left\{\frac{m(m+1)}{R^{m+2}}(a_2 - a_{20}) + \frac{m}{R^2}(b - b_0)[xH_{m-1} - (m+1)H_m]\right\} = \rho_1 R^m\left(\ddot{a}_1 + g\frac{m}{R}a_1\right), \quad (29)$$

where $a_0 = a(0)$ and $b_0 = b(0)$. In addition, in the above equations and hereafter $x$ denotes its value on the interface, that is, $x = q_m R$. We also notice that in obtaining these equations we have used the recurrence formulas for the Hankel function

$$H'_m = H_{m-1} - \frac{m}{x}H_m, \quad (30)$$

$$H'_{m-1} = \frac{m-1}{x}H_{m-1} - H_m, \quad (31)$$

where $H'_m$ denotes the derivative of $H_m$ with respect to the argument $x$. In addition, we have introduced the constant $C_0$ in Eq. (29) by taking into account the incomplete definition of the potentials $\phi_n$ in order to impose the conditions of being stress-free and of the irrotationality of the displacement field as initial conditions, since we are considering that vorticity is created by the elasticity effects at times $t > 0$. Then, after a short calculation, we get the equation of motion for the perturbation oscillations at the interface,

$$\left(\ddot{\xi} - A_T\frac{m}{R}\xi\right)(xH_m + 2H_{m-1}) = m(m+1)\frac{(1+A_T)G}{\rho_2 R^2}H_{m-1}\left\{xH_m\frac{\ddot{\xi} - \ddot{\xi}_0}{\omega_{mj}^2} - [xH_m - 2(m-1)H_{m-1}](\xi - \xi_0)\right\}, \quad (32)$$

where $\ddot{\xi}_0 = \ddot{\xi}(0)$, $\xi_0 = \xi(0)$, and $A_T = (\rho_2 - \rho_1)/(\rho_2 + \rho_1)$ is the Atwood number. We notice that the above dispersion relation is analogous to the one obtained in Ref. [48] with the Hankel function of the first kind $H_m$ instead of the modified Bessel function of the second kind $K_m$.

The general solution of Eq. (32) can be constructed in the usual manner by adding the solution of the homogeneous part to a particular solution of the complete equation. The solution of the homogeneous part is found by proposing an exponential solution of the form $e^{i\omega_{mj}t}$. In this manner, the homogeneous part of Eq. (32) leads to the dispersion relation for the oscillation frequencies $\omega_{mj}$:

$$\left(\omega_{mj}^2 + A_T\frac{m}{R}g\right)(xH_m + 2H_{m-1}) = m(m+1)\frac{(1+A_T)G}{\rho_2 R^2}[xH_m - 2(m-1)H_{m-1}]. \quad (33)$$

Since the Hankel function is given by Eq. (19), Eq. (33) actually yields two equations corresponding, respectively, to the real and imaginary parts of $H_m$. However, since $J_m(x) \to 0$ for $x \to 0$, we can see that only the imaginary part yields a physically meaningful equation that leads to the same result as the unstable solution in the cutoff, when $\omega_{mj} = 0$. In fact, in such a limit $xY_m(x), Y_{m-1}(x) \to 2(m-1)$ and we retrieve the cutoff value $B_c$ for the dimensionless radius $B = \rho_2 gR/G$, already found in Ref. [48] for the unstable regime:

$$B_c = \frac{1+A_T}{A_T}\frac{m^2-1}{m}. \quad (34)$$

Then the equation of motion for the perturbation oscillations is given by Eq. (32) by identifying $H_m$ with the Bessel function of the second kind $Y_m$. On the other hand, we can write the dispersion relation (33) in the convenient form

$$\frac{\Omega_m^2(x)}{\sigma_p^2} = \frac{1}{\Lambda_m(x)} - 1, \quad x = \Omega_m B, \quad (35)$$

where the definitions for the dimensionless magnitudes have been introduced,

$$\Omega_m^2 = \omega_{mj}^2\left(\frac{G}{\rho_2 g^2}\right), \quad \sigma_p^2 = A_T\frac{m}{R}g\left(\frac{G}{\rho_2 g^2}\right), \quad (36)$$

$$\Lambda_m(x) = \frac{A_T B}{2(1+A_T)(m+1)}\frac{F_m(x)+2}{F_m(x) - m + 1}, \quad (37)$$

where

$$F_m(x) = \frac{xY_m(x)}{Y_{m-1}(x)}. \quad (38)$$

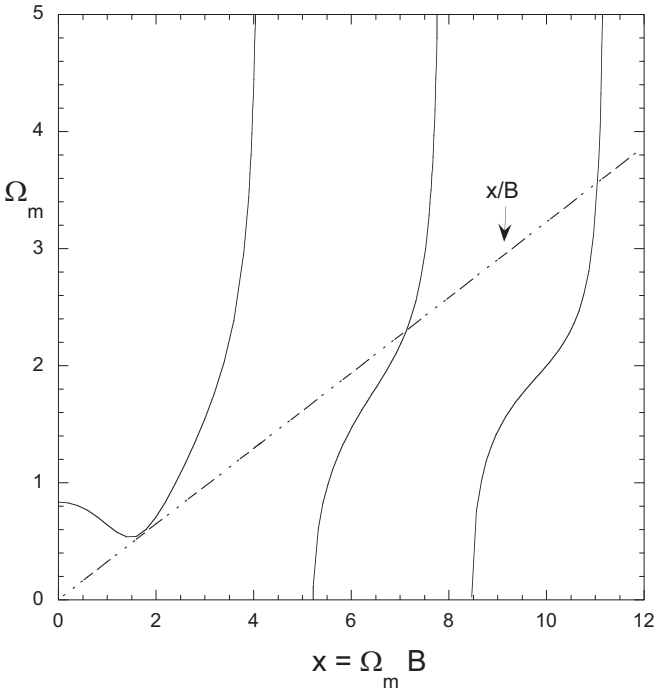


FIG. 2. Dimensionless frequency $\Omega_m(x)$ and $x/B$ given by Eq. (35) for $A_T = 1$, $m = 3$, and $B = 3.1$.

In Fig. 2 we represent $\Omega_m(x)$ and $x/B$ as given by Eq. (35) for a typical case with $A_T = 1$, $m = 3$, and $B = 3.1$ in order to show how the different solutions result from the intersection of the straight line with the different branches of the function $\Omega_m(x)$ giving place to an infinite number of oscillations frequencies.

As it was discussed in Refs. [31,35], for the purpose of finding the stability boundaries, we are interested in the lowest frequency, that is, the one imposing the most restrictive conditions on the stability of the interface and which describes the average evolution of the perturbation oscillations. This lowest frequency $\omega_m$, in dimensionless form $\Omega = \omega_m\sqrt{G/\rho_2 g^2}$, is represented in Fig. 3 as a function of the dimensionless radius $B$ of the cylindrical interface for several modes $m$ ($m = 2$, 4, 6, and 8) and for two values of the Atwood number ($A_T = 1$ and 0.3). In every case $\Omega(B)$ presents a discontinuity that corresponds to the jump from the second to the first branch of $\Omega_m(x)$ (Fig. 2) as $B$ is increased, with the consequent reduction of the lowest frequency and making the system less stable. Figure 3 is in a semilogarithmic scale to make this jump more evident, which later will be reflected in the boundaries of stability. The results are qualitatively the same for the different Atwood numbers but, as it could be expected, for any particular spatial mode $m$, the cutoff value $B_c$ [$\Omega(B_c) = 0$] of the dimensionless radius [Eq. (34)] is larger for the smaller values of $A_T$, showing a wider range of stability. In addition, we can also notice that the magnitude of the jump decreases for the largest modes $m$.

### B. Plastic phase

As in the previous studies for the planar case [31,35], we assume the classical theory of plasticity in which the

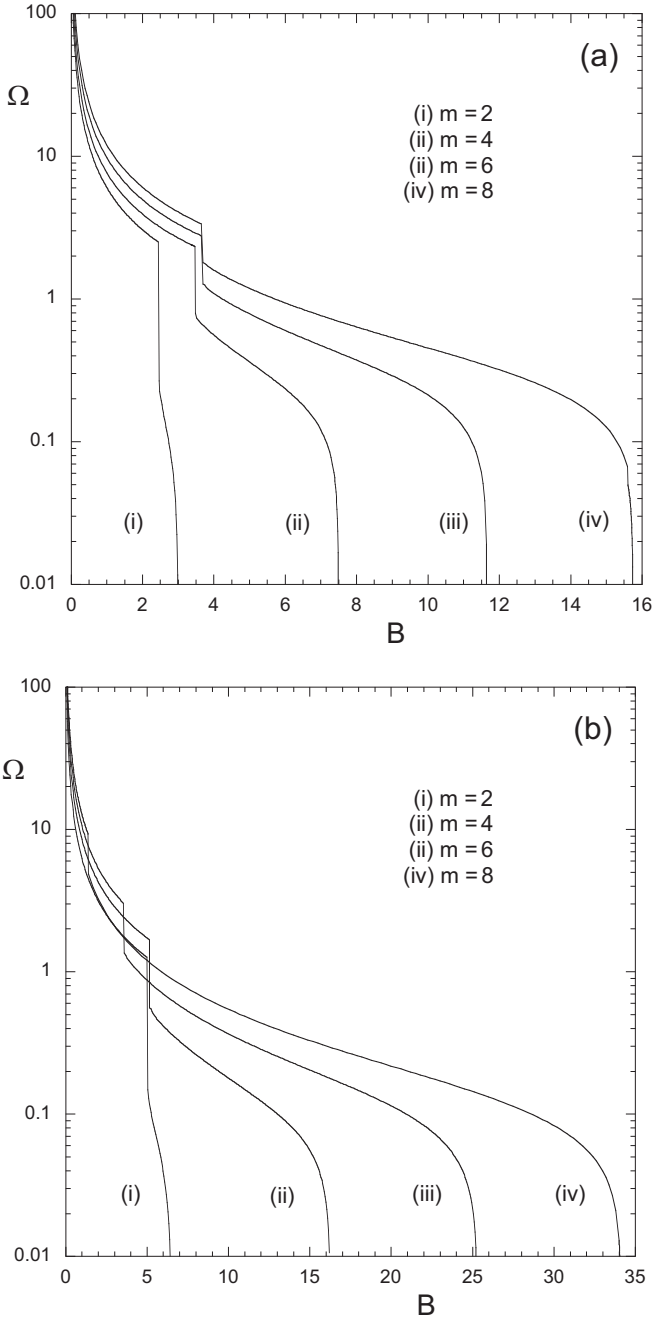


FIG. 3. Dimensionless lowest frequency $\Omega$ as a function of the dimensionless radius $B$ for several modes $m$, (i) $m = 2$, (ii) $m = 4$, (iii) $m = 6$, and (iv) $m = 8$, with (a) $A_T = 1$ and (b) $A_T = 0.3$..

displacement field is assumed to be irrotational [36]. Therefore, it is $\psi_2 = 0$ and from Eq. (14) we get

$$\frac{\dot{\vec{e}}}{\|\dot{\vec{e}}\|} = \frac{\cos m\theta}{\sqrt{3}}. \tag{39}$$

On the other hand, as it was already discussed, the transition to the RTI regime controlled by the plasticity does not occur just when the von Mises flow criterion is satisfied, but somewhat later when a considerable region of the solid becomes plastic and the plastic collapse occurs [50,51]. Then

we consider that, for the transition to occur, the stress must reach a value

$$S_{rr} = \frac{\beta Y}{\sqrt{3}} \cos m\theta, \quad \beta > 1. \tag{40}$$

In analogy with the planar case, for quantitative calculations we will take $\beta \sim 3$ ($\beta/\sqrt{3} \sim 2$). Then, from Eq. (24) we get

$$\ddot{\xi} - A_T \frac{m}{R} g\xi = -\frac{\beta(1+A_T)m}{2\sqrt{3}\rho_2 R} Y. \tag{41}$$

As in the elastic case, the general solution of this equation can be constructed as the solution of the homogeneous part plus a particular solution. The solution of the homogeneous part is obtained by proposing the exponential form $\xi \propto e^{\gamma_p t}$, where $\gamma_p$ is the instability growth rate during the elastic phase, and it ends up being just the one corresponding to the classical RTI case:

$$\gamma_p^2 = A_T \frac{m}{R} g. \tag{42}$$

## III. BOUNDARIES OF STABILITY

As it was shown in Ref. [20], the necessary condition for the stability of the system is that it must be stable during the elastic phase described by Eqs. (32) and (33). Since Eq. (33) has an infinite number of roots for each mode $m$, the general solution will consist in oscillations containing an infinite number of frequencies. Indeed, the solution of Eq. (32) can be considered like an oscillation with the lowest frequency, which leads to the most unstable situation, plus an infinite number of superposed modes of oscillation with higher frequencies [31,35]. Therefore, for times shorter than the transition time $t_T$, from the RTI regime controlled by the elasticity to the one controlled by the plasticity, the average evolution of the perturbations is described by the equation

$$z = 1 + \frac{\ddot{\xi}_0}{\xi_0 \omega_m^2}(1 - \cos \Omega\tau), \tag{43}$$

where the lowest frequency $\omega_m$ and its dimensionless form $\Omega$ are given by Eq. (35). In addition, the following definitions have been used:

$$z = \frac{\xi}{\xi_0}, \quad \tau = t\sqrt{\frac{\rho_2 g^2}{G}}. \tag{44}$$

The initial acceleration $\ddot{\xi}_0$ can be obtained from Eq. (32) by evaluating it at $t = 0$:

$$\frac{\ddot{\xi}_0}{\xi_0 \omega_m^2} = \frac{\sigma_p^2}{\Omega^2}. \tag{45}$$

On the other hand, for times $t \geqslant t_T$, when the system achieves the regime of unrestricted plastic flow, the perturbation evolution is described by the solution of Eq. (41),

$$z = \frac{1}{\xi^*} + K_1 e^{\sigma_p \tau} + K_2 e^{-\sigma_p \tau}, \tag{46}$$

where

$$\xi^* = \frac{2\sqrt{3}A_T}{1+A_T} \frac{\rho_2 g \xi_0}{\beta Y} \tag{47}$$

and $K_1$ and $K_2$ are constants to be determined from the matching conditions with Eq. (43) at the transition time $t_T$.

We also notice that at $t = t_T$ we have, from Eq. (43),

$$\ddot{\xi}_T - \ddot{\xi}_0 = -\omega_m^2(\xi_T - \xi_0), \tag{48}$$

where $\ddot{\xi}_T = \ddot{\xi}(t_T)$. Therefore, from Eqs. (32) and (41) and using Eqs. (37) and (48), we can write

$$z_T - 1 = \frac{\Lambda}{\xi^*}, \tag{49}$$

with $\Lambda$ denoting the corresponding value of $\Lambda_m$ for the lowest frequency $\Omega$. Then, from Eq. (43) it turns out that

$$\cos \Omega\tau_T = 1 - \frac{\Omega^2}{\sigma_p^2} \frac{\Lambda}{\xi^*}. \tag{50}$$

Now the constants $K_1$ and $K_2$ can be determined from Eqs. (43) and (46) by noticing that at $t = t_T$ the perturbation amplitude $\xi(t_T) = \xi_T$ and velocity $\dot{\xi}(t_T) = \dot{\xi}_T$ must be continuous. Thus, it turns out

$$K_1 e^{\sigma_p \tau_T} + K_2 e^{-\sigma_p \tau_T} = 1 + \frac{\Lambda - 1}{\xi^*}, \tag{51}$$

$$K_1 e^{\sigma_p \tau_T} - K_2 e^{-\sigma_p \tau_T} = \frac{\sigma_p}{\Omega} \sin \Omega\tau_T, \tag{52}$$

and solving for $K_1$ and $K_2$ we get

$$2K_2 e^{-\sigma_p t} = 1 + \frac{\Lambda - 1}{\xi^*} - \frac{\sigma_p}{\Omega} \sin \Omega\tau_T, \tag{53}$$

$$2K_1 e^{\sigma_p t} = 1 + \frac{\Lambda - 1}{\xi^*} + \frac{\sigma_p}{\Omega} \sin \Omega\tau_T. \tag{54}$$

As in Refs. [20,31,35] we need to impose conditions for the marginal stability by taking into account that the interface will be stable provided the perturbation amplitude reaches an absolute maximum at a certain time $t = t_m \geqslant t_T$. Then it must be that $\dot{\xi}(t_m) = 0$ and $\ddot{\xi}(t_m) \leqslant 0$, and the marginal stability conditions, in dimensionless form, read

$$\dot{z}(\tau_m) = 0, \quad \ddot{z}(\tau_m) = 0 \quad (\tau_m \geqslant \tau_T). \tag{55}$$

These conditions can only be satisfied when the system is stable in the purely elastic phase. Therefore, we apply the previous marginal stability conditions to the plastic regime evolution described by Eq. (46) [with $K_1$ and $K_2$ given by Eqs. (53) and (54), respectively]. Since Eqs. (55) can only be satisfied when $K_2 = 0$, the equation for the dimensionless amplitude $\xi_{th}^*$ under marginal stability conditions results in

$$1 + \frac{\Lambda - 1}{\xi_{th}^*} = \frac{\sigma_p}{\Omega} \sqrt{1 - \left(1 - \frac{\Omega^2}{\sigma_p^2} \frac{\Lambda}{\xi_{th}^*}\right)^2}, \tag{56}$$

where we have used Eq. (50). Furthermore, using Eq. (35) and after a short calculation, the previous expression takes a much simpler form

$$\xi_{th}^* = 1 - \sqrt{\Lambda} \tag{57}$$

$$or \xi_{th}^* = 1 - \frac{\sigma_p}{\sqrt{\sigma_p^2 + \Omega^2}}. \tag{58}$$

The form given by Eq. (57) is analogous to the one found in Ref. [20] for the marginal stability conditions in planar geometry with semi-infinite media. In that case $\Lambda$ represented

the dimensionless perturbation wavelength $\lambda^* = \rho_2 g\lambda/4\pi G$. In the present case, instead, it is $\Lambda = \Lambda(A_T, B, m)$, which must be determined from the roots of Eq. (35).

In the same manner we can easily obtain the equation for the EP transition by requiring that the perturbation amplitude $z_T$ at the transition be reached when, in the elastic regime, the oscillation amplitude is a maximum. That is, when $z^{\max} = z_T$, it turns out that

$$\frac{2\sigma_p^2}{\Omega^2} = \frac{\Lambda}{\xi_{EP}^*}, \tag{59}$$

where we have used Eqs. (43), (45), and (49). Then, from Eq. (35) we get

$$\xi_{EP}^* = \tfrac{1}{2}(1 - \Lambda), \tag{60}$$

which also resembles the result of Ref. [20] for the planar case by changing $\lambda^* \to \Lambda$. From Eqs. (60) and (57), the relationship between $\xi_{EP}^*$ and $\xi_{th}^*$ can be written

$$\xi_{EP}^* = \tfrac{1}{2}[1 - (1 - \xi_{th}^*)^2], \tag{61}$$

which once again indicates the feature previously noticed in Ref. [20] that $\xi_{EP}^* \leqslant \xi_{th}^*$ and therefore the transition to the plastic regime must in general occur before the system becomes unstable. Thus, plastic flow is necessary for instability but not at all sufficient and in general there exists a regime of stability after plastic flow has occurred.

## IV. RESULTS AND DISCUSSION

In Fig. 4 represent the stability boundaries $\xi_{th}^* = \xi_{th}^*(B, A_T, m)$ as given by Eqs. (57) and (35)–(38), as a function of the dimensionless radius $B$ of the cylindrical surface, for two values of the Atwood number ($A_T = 1$ and 0.3) and for several modes $m$ ($m = 2, 4, 6, 8$). As it could be expected, the different curves for marginal stability present a jump that reflects the behavior observed in Fig. 3 for the lowest oscillation frequency. This jump decreases in magnitude as the mode $m$ increases and, for the largest values of $m$, it moves towards the smallest values of $B$. At the limit of very large values of $m$, the oscillation frequency $\Omega$ becomes determined only by the second branch of $\Omega(x)$ in Fig. 2.

In order to explain these features we notice that, since the stable region for $B < B_c$ exists because the system is stable in the initial elastic phase, it depends on the stable solutions of the dispersion relation. As we have already discussed, in such a stable regime, the system oscillates with multiple infinite frequency modes. However, the most stringent requirement for the stability is set by the lowest oscillation frequency. This is because the oscillation with the lowest frequency describes the average evolution of the multifrequency oscillation. These facts are independent of the geometry of the system and are also present in planar geometry [31]. However, in cylindrical geometry, the curvature effects introduce the radius $R$ as a new characteristic length. Therefore, for large values of $R$, the system behaves like in planar geometry and the characteristic oscillation frequency is determined by the only relevant characteristic length, the perturbation wavelength. However, when $R$ is small enough and it becomes another significant characteristic length, a new branch with different traits appears such as that shown in Fig. 2 for the lowest values of $x$. This

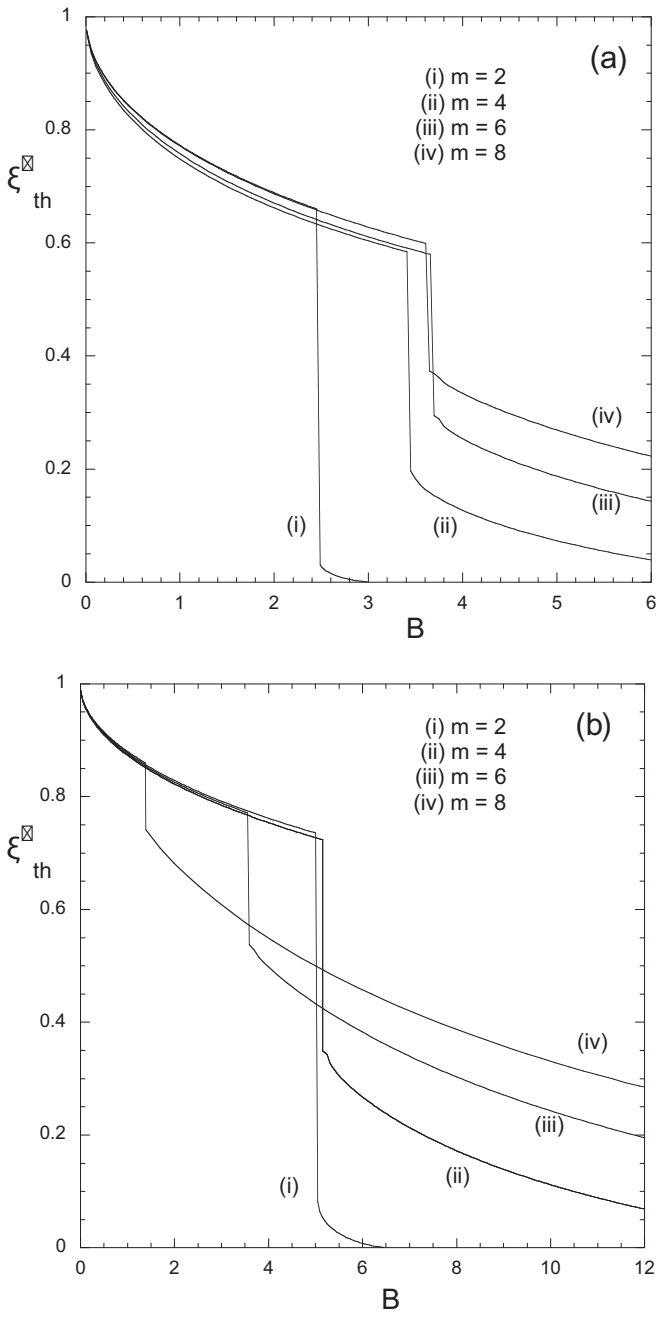


FIG. 4. Stability boundaries $\xi_{th}^*(B)$ for several modes $m$, (i) $m = 2$, (ii) $m = 4$, (iii) $m = 6$, and (iv) $m = 8$, with (a) $A_T = 1$ and (b) $A_T = 0.3$.

branch determines a new lowest oscillation frequency that is larger than the one determined by the wavelength. In addition, this change of behavior is not continuous when $R$ is reduced because stable situations ($\Omega_m > 0$) can only exist for certain ranges of values of $x$ corresponding to the different branches in Fig. 2. The ranges in between of course correspond to unstable situations. Therefore, there is a discontinuous change in the lowest oscillation frequency when we go from one stable region to other and it gives place to the observed jump shown in Fig. 3. As it can be appreciated in Figs. 3 and 4, the effect of such a branch enhances the stability region for the smallest

radii $R$, but it also becomes less and less relevant as the mode $m$ increases and the system approaches the planar limit.

From Eqs. (57) and (58) we can see that $0 \leqslant \xi_{th}^* \leqslant 1$. In fact, in the cutoff, when $\Omega = 0$ ($x = \Omega B = 0$), we have $B = B_c$, $\Lambda = 1$, and $\xi_{th}^* = 0$. As it was already mentioned, this limit is determined exclusively by the elastic properties of the medium since for $B \geqslant B_c$ the system is already unstable in the early elastic regime.

At the other extreme, when $B = 0$ ($x = 0$), we have $\Lambda = 0$ and $\xi_{th}^* = 1$ for any value of $m$. Then, from Eq. (47) we find that the cylindrical geometry equivalent to Drucker's criterion reads [49,50]

$$\frac{2\sqrt{3}A_T}{1+A_T}\frac{\rho_2 g\xi_0}{\beta Y} = 1. \tag{62}$$

Drucker's criterion was originally obtained for the RTI in purely rigid plastic media at a planar interface with $A_T = 1$ and it is valid in the limit of very short perturbation wavelengths ($\lambda = 0$). However, as it can be seen, in cylindrical geometry we find the same result in the limit when $\Lambda = 0$ ($B = 0$), such that it could be expected from the role of the parameter $\Lambda$ in Eq. (57) as the equivalent of the perturbation wavelength in planar geometry (note that the number of wavelengths that can be accommodated in the perimeter $2\pi R$ of interface is just $\lambda = 2\pi R/m$).

This coincidence has nothing to do with the planar limit of the cylindrical problem, which indeed corresponds to the opposite limit ($B \gg 1$). Instead, it is related to the physical meaning of Eq. (62), which, as it was shown by Drucker, is also valid for a single bump with a high of the order of $\xi_0$. In fact, it just reflects the feature that the plastic collapse will occur when the weight per unitary area $\rho_2 g\xi_0$ overcomes the yield strength $Y$ and it is therefore independent of the interface geometry. This condition also coincides with the one usually considered to estimate the maximum possible high of a mountain either on earth or on a neutron star, which marks the maximum weight that can be supported by the crust [54]. For the intermediate values of $B$ ($0 < B < B_c$) in which the system is stable in the elastic regime, it is still stable after plastic flow takes place [determined by Eq. (61) for the EP transition] provided the initial perturbation amplitude remains below the marginal stability curve.

The stability boundaries given in Fig. 4 show that the maximum amplitude that can be tolerated by the system without being unstable decreases with the parameter $B$ for any mode $m$ and that this amplitude becomes equal to zero for the cutoff value $B_c$ of the parameter. This is because the region with $B \leqslant B_c$ corresponds to situations in which the system is stable during the initial elastic phase and therefore it can remain stable provided the initial amplitude is not too large. For $B > B_c$ the system is already unstable in the elastic regime and thus it will never be stable independently of the value of the initial amplitude $\xi_0$.

In this sense, the stability boundaries represented in Fig. 4, and compactly expressed by Eq. (57), can be considered as a generalization of Drucker's criterion for arbitrary values of $\Lambda$, thus including the effects of elasticity (EP media) and of the interface geometry. In fact, the Drucker criterion is not valid when elasticity is present, and in such an unphysical situation there is no cutoff value for the parameter $B$ ($B_c \to \infty$). Then the stability boundary is determined only by the initial perturbation amplitude $\xi_0$ such as that given by Eq. (62). However, when the unavoidable elastic initial phase is taken into account, it imposes an extra restriction that reduces the maximum allowable initial amplitude of the perturbations according to the corresponding value of $B$. Beyond the cutoff, the system will be unstable for any value of $\xi_0$ because, as we have already mentioned, the initial elastic phase is already unstable.

It may also be worth noting that the initial elastic phase is unavoidable and thus it will be always present. In fact, even in the case when the material in the unperturbed state has been taken in some manner to the plastic state, the onset of the instability will occur by growing initially in the elastic phase. This is because the plastic state can only exist under the action of a sustained deformation rate and it immediately relaxes to a new elastic state under the onset of any small perturbation.

As it was previously noticed in Ref. [48], for the lowest mode $m = 1$, the cutoff value of $B$ given by Eq. (34) becomes $B_c = 0$ and the mechanical properties of the solid are unable to stabilize this mode no matter how small the perturbation amplitude is. However, for the particular case of the LAPLAS experiment discussed in the Introduction, this mode can be stabilized by the rotating beam that creates the annular focal spot by means of which the absorber region that surrounds the solid pusher is heated by the ion beam. In fact, the wobbler system that rotates the beam is being designed to produce an asymmetry level below 1–2 % [55], and it has been shown that the mode $m = 1$ can be canceled provided a suitable noninteger number of beam revolutions is performed by the wobbler [56]. Therefore, while the higher modes would be stabilized by the mechanical properties of the pusher material, the lowest mode could be stabilized by a suitable operation of the rotating beam.

In fact, in LAPLAS, extensive numerical simulations show that, depending on the sample at the interior of the shell (Fe, $H_2O$, and $H_2$), the Atwood number is $0.3 \leqslant A_T \leqslant 1$, the radius at the implosion stagnation is $R \leqslant 200$ $\mu$m, and $g \approx 10^{10}$ m/s$^2$ [37–44]. Since the shell is made of Ta, we can take $G \approx 160$ GPa and $Y = 2.2$ GPa [57], and for these values it turns out that $B < 1$. Therefore, according to the results shown in Fig. 4, the interface would be stabilized by the pusher elastic-plastic mechanical properties for all the modes $m > 1$ provided that $\xi_{th}^* \lesssim 0.5$–$0.6$.

For the typical values mentioned above, the required initial amplitude $\xi_0$ at the beginning of the stagnation phase should be less than 10–20 $\mu$m. This value will be actually determined by the previous implosion phase dominated by the Bell-Plesset effects that depend on the convergence of the interface and the compressibility of the media [58]. So more precise estimations would require the analysis of the Bell-Plesset effects, which is beyond the scope of the present work.

## V. CONCLUSION

On the basis of the methodological procedure developed in Refs. [31,35] for the planar geometry RTI, we have extended the previous results to the case of a cylindrical interface in

order to shed light on the conditions for marginal stability determined by the mechanical properties at the stagnation phase of a cylindrical implosion, like the one considered in the LAPLAS experimental setup.

As in the case of planar geometry RTI, plastic flow results to be necessary for instability, but is not sufficient. After the EP transition has occurred, a stable plastic region generally exists that determines the maximum initial perturbation amplitude that keeps the system stable for any particular value of the dimensionless radius $B$ of the interface (for a given spatial mode $m$ and Atwood number $A_T$).

The effects of the interface curvature, expressed by the dimensionless radius $B$, are seen to make the system more stable for a smaller radius, in the sense that the interface can tolerate larger initial amplitudes of the perturbations. This is true essentially for all the modes $m > 1$ but, as it was already noticed in Ref. [48], the mechanical properties of the pusher cannot stabilize the lowest mode $m = 1$. In the case of LAPLAS, the wobbler system that will generate the annular focal spot can be conveniently operated to cancel such a mode just by producing a noninteger number of revolutions of the rotating beam [56].

Since the initial amplitude $\xi_0$ at the stagnation phase will be determined by the previous implosion phase dominated by the Bell-Plesset effects, including the effects of the geometrical convergence and compressibility of the involved media [58], as well as by the quality of the surface finish of the interface and by the feedthrough effect of RTI at the outer surface of the shell, it is difficult to provide a good estimation of $\xi_0$. However, the present work allows for putting a limit on the maximum initial amplitude that can be tolerated in order to have a stable stagnation phase.

## ACKNOWLEDGMENTS

This work was partially supported by the Junta de Comunidades de Castilla–La Mancha of Spain (Grant No. SBPLY/17/180501/000264) and by the BMBF of Germany.

[1] N. A. Tahir, D. H. H. Hoffmann, J. A. Maruhn, P. Spiller, and R. Bock, Phys. Rev. E **60**, 4715 (1999).
[2] C. A. Hall, J. R. Asay, M. D. Knudson, W. A. Stygar, R. B. Spielman, T. D. Pointon, D. B. Reisman, A. Toor, and R. C. Cauble, Rev. Sci. Instrum. **72**, 3587 (2001).
[3] J-P. Davis, C. Deeney, M. D. Knudson, R. W. Lemke, T. D. Pointon, and D. E. Bliss, Phys. Plasmas **12**, 056310 (2005).
[4] R. E. Reinovsky, W. E. Anderson, W. L. Atchison, C. E. Ekdahl, R. J. Faehl, I. R. Lindemuth, D. V. Morgan, M. Murillo, J. L. Stokes, and J. S. Shlachter, IEEE Trans. Plasma Sci. **30**, 1764 (2002).
[5] S. M. Bakhrakh, O. B. Drennov, N. P. Kovalev, A. I. Lebedev, E. E. Meshkov, A. L. Mikhailov, N. V. Neumerzhitsky, P. N. Nizovtsev, V. A. Rayevsky, G. P. Simonov, V. P. Solovyev, and I. G. Zhidov, Lawrence Livermore National Laboratory Report No. UCRL-CR-126710, 1997 (unpublished), available at https://www.osti.gov/scitech/servlets/purl/515973.
[6] J. R. Davies, D. H. Barnak, R. Betti, E. M. Campbell, P.-Y. Chang, A. B. Sefkow, K. J. Peterson, D. B. Sinars, and M. R. Weis, Phys. Plasmas **24**, 062701 (2017).
[7] S. Opie, E. Loomis, P. Peralta, T. Shimada, and R. P. Johnson, Phys. Rev. Lett. **118**, 195501 (2017).
[8] P. F. Knapp, M. R. Martin, D. H. Dolan, K. Cochrane, D. Dalton, J.-P. Davis, C. A. Jennings, G. P. Loisel, D. H. Romero, I. C. Smith, E. P. Yu, M. R. Weis, T. R. Mattsson, R. D. McBride, K. Peterson, J. Schwarz, and D. B. Sinars, Phys. Plasmas **24**, 042708 (2017).
[9] J. F. Barnes, P. J. Blewet, R. G. McQueen, K. A. Meyer, and D. Venable, J. Appl. Phys. **45**, 727 (1974).
[10] J. F. Barnes, D. H. Janney, R. K. London, K. A. Meyer, and D. H. Sharp, J. Appl. Phys. **51**, 4678 (1980).
[11] J. W. Swegle and A. C. Robinson, J. Appl. Phys. **66**, 2838 (1989).
[12] A. C. Robinson and J. W. Swegle, J. Appl. Phys. **66**, 2859 (1989).
[13] G. Dimonte, R. Gore, and M. Schneider, Phys. Rev. Lett. **80**, 1212 (1998).
[14] D. H. Kalantar, B. A. Remington, J. D. Colvin, K. O. Mikaelian, S. V. Weber, L. G. Wiley, J. S. Wark, A. Loveridge, A. M. Allen, A. A. Hauer, and M. A. Meyers, Phys. Plasmas **7**, 1999 (2000).
[15] J. D. Colvin, M. Legrand, B. A. Remington, G. Shurtz, and S. V. Weber, J. Appl. Phys. **93**, 5287 (2003).
[16] K. T. Lorenz, M. J. Eswards, S. G. Glendinning, A. F. Jankowski, J. McNaney, S. M. Pollaine, and B. A. Remington, Phys. Plasmas **12**, 056309 (2005).
[17] B. A. Remington, P. Allen, E. M. Bringa, J. Hawreliak, D. Ho, K. T. Lorenz, H. Lorenzana, J. M. McNaney, M. A. Meyers, S. W. Pollaine, K. Rosolankova, B. Sadik, M. S. Schneider, D. Swift, J. Wark, and B. Yaakobi, Mater. Sci. Technol. **22**, 474 (2006).
[18] H. S. Park, K. T. Lorenz, R. M. Cavallo, S. M. Pollaine, S. T. Prisbrey, R. E. Rudd, R. C. Becker, J. V. Bernier, and B. A. Remington, Phys. Rev. Lett. **104**, 135504 (2010).
[19] J. W. Miles, General Dynamics Report No. GAMD-7335, AD 643161, 1966 (unpublished).
[20] A. R. Piriz, J. J. López Cela, and N. A. Tahir, Phys. Rev. E **80**, 046305 (2009).
[21] J. J. López Cela, A. R. Piriz, M. C. Serna Moreno, N. A. Tahir, and D. H. H. Hoffmann, Laser Part. Beams **24**, 427 (2006).
[22] B. J. Plohr and D. H. Sharp, Z. Angew. Math. Phys. **49**, 786 (1998).
[23] G. Terrones, Phys. Rev. E **71**, 036306 (2005).
[24] G. Terrones, J. Appl. Phys **102**, 034908 (2007).
[25] A. R. Piriz, J. J. López Cela, M. C. Serna Moreno, N. A. Tahir, and D. H. H. Hoffmann, Laser Part. Beams **24**, 275 (2006).
[26] S. A. Piriz, A. R. Piriz, and N. A. Tahir, Phys. Rev. E **95**, 053108 (2017).
[27] S. A. Piriz, A. R. Piriz, and N. A. Tahir, Phys. Rev. E **96**, 063115 (2017).
[28] S. A. Piriz, A. R. Piriz, and N. A. Tahir, Phys. Rev. E **97**, 043106 (2018).

[29] S. A. Piriz, A. R. Piriz, and N. A. Tahir, J. Fluid Mech. **867**, 1012 (2019).
[30] S. A. Piriz, A. R. Piriz, and N. A. Tahir, Phys. Fluids **30**, 111703 (2018).
[31] A. R. Piriz, S. A. Piriz, and N. A. Tahir, Phys. Rev. E **100**, 063104 (2019).
[32] S. Mora, T. Phou, J.-M. Fromental, and Y. Pomeau, Phys. Rev. Lett. **113**, 178301 (2014).
[33] I. Maimouni, J. Goyon, E. Lac, T. Pringuey, J. Boujlel, X. Chateau, and P. Coussot, Phys. Rev. Lett. **116**, 154502 (2016).
[34] R. Polavarapu, P. Roach, and A. Banerjee, Phys. Rev. E **99**, 053104 (2019).
[35] S. A. Piriz, A. R. Piriz, N. A. Tahir, S. Richter, and M. Bestehorn, Phys. Rev. E **103**, 023105 (2021).
[36] M. E. Gurtin and L. Anand, J. Mech. Phys. Solids **52**, 2425 (2004).
[37] N. A. Tahir, V. Kim, A. Matvechev, A. Ostrik, A. V. Shutov, I. V. Lomonosov, A. R. Piriz, J. J. López Cela, and D. H. H. Hoffmann, Nucl. Instrum. Methods Phys. Res. Sect. B **245**, 85 (2006).
[38] N. A. Tahir, I. V. Lomonosov, B. Borm, A. R. Piriz, P. Neumayer, A. Shutov, V. Bagnoud, and S. A. Piriz, Contrib. Plasma Phys. **57**, 493 (2017).
[39] N. A. Tahir, P. Neumayer, I. V. Lomonosov, A. Shutov, V. Bagnoud, A. R. Piriz, S. A. Piriz, and C. Deutsch, Phys. Rev. E **101**, 023202 (2020).
[40] N. A. Tahir, I. V. Lomonosov, B. Borm, A. R. Piriz, A. Shutov, P. Neumayer, V. Bagnoud, and S. A. Piriz, Astrophys. J. Suppl. **232**, 1 (2017).
[41] N. A. Tahir, A. Shutov. I. V. Lomonosov, A. R. Piriz, P. Neumayer, V. Bagnoud, and S. A. Piriz, Astrophys. J. Suppl. **238**, 27 (2018).
[42] N. A. Tahir, P. Neumayer, A. Shutov, A. R. Piriz, I. V. Lomonosov, V. Bagnoud, S. A. Piriz, and C. Deutsch, Contrib. Plasma Phys. **59**, e201800143 (2019).
[43] N. A. Tahir, A. Shutov, A. R. Piriz, P. Neumayer, I. V. Lomonosov, V. Bagnoud, and S. A. Piriz, Contrib. Plasma Phys. **59**, e201800135 (2019).
[44] N. A. Tahir, A. Shutov, P. Neumayer, V. Bagnoud, A. R. Piriz, I. V. Lomonosov, and S. A. Piriz, Phys. Plasmas **28**, 032712 (2021).
[45] G. Terrones and M. D. Carrara, Phys. Fluids **27**, 054105 (2015).
[46] G. Terrones and T. Heberling, Phys. Fluids **32**, 094105 (2020).
[47] S. Chandrasekhar, Q. J. Mech. Appl. Math. **8**, 1 (1955).
[48] Y. B. Sun, R. H. Zeng, and J. J. Tao, Phys. Plasmas **28**, 062701 (2021).
[49] D. C. Drucker, in *Mechanics Today*, edited by S. Nemmat-Nasser (Pergamon, Oxford, 1980), Vol. 5, p. 37.
[50] D. C. Drucker, Ing. Arch. **49**, 361 (1980).
[51] W. F. Chen, *Limit Analysis and Soil Plasticity* (Elsevier, Amsterdam, 1975).
[52] M. Abramowitz and I. A. Stegun, *Handbook of Mathematical Functions: With Formulas, Graphs, and Mathematical Tables* (Dover, New York, 1965).
[53] A. C. Eringen and E. S. Şuhubi, *Elastodynamics* (Academic, New York, 1975), Vol. II.
[54] P. A. G. Scheuer, J. Astrophys. Astron. **2**, 165 (1981).
[55] A. R. Piriz, M. Temporal, J. J. López Cela, N. A. Tahir, and D. H. H. Hoffmann, Plasma Phys. Control. Fusion **45**, 1733 (2003).
[56] A. Bret, A. R. Piriz, and N. A. Tahir, Phys. Rev. E **85**, 036402 (2012).
[57] D. J. Steinberg, S. G. Cochran, and M. W. Guinan, J. Appl. Phys. **51**, 1498 (1980).
[58] R. Epstein, Phys. Plasmas **11**, 5114 (2004).